Article

Not peer-reviewed version

Piezoelectric and Pyroelectric Properties of Organic MDABCO-NH4Cl3 Perovskite for Flexible Energy Harvesting

Rosa M. F. Baptista *, Bruna Silva, João Oliveira, Bernardo Almeida, Cidália Castro, Pedro V. Rodrigues, Ana Machado, Etelvina de Matos Gomes, Michael Belsley *

Posted Date: 7 February 2024

doi: 10.20944/preprints202402.0436.v1

Keywords: organic perovskite; electrospinning; fibers; piezoelectricity; pyroelectricity; nano energy harvesting

Article

Piezoelectric and Pyroelectric Properties of Organic MDABCO-NH_4Cl_3 Perovskite for Flexible Energy Harvesting

Rosa M. F. Baptista [1,*], Bruna Silva [1], João Oliveira [1], Bernardo Almeida [1], Cidália Castro [2], Pedro V. Rodrigues [2], Ana Machado [2], Etelvina de Matos Gomes [1] and Michael Belsley [1,*]

[1] Centre of Physics of Minho and Porto Universities (CF-UM-UP), Laboratory for materials and Emergent Technologies (LAPMET), University of Minho, Campus de Gualtar, 4710-057 Braga, Portugal; brunasilva@fisica.uminho.pt (B.S.); b8171@fisica.uminho.pt (J.O.); bernardo@fisica.uminho.pt (B.A.); emg@fisica.uminho.pt (E.d.M.G.)

[2] Institute for Polymers and Composites, University of Minho, Campus de Azurém, 4800-058 Guimarães, Portugal; cidaliacastro@dep.uminho.pt (C.C.); pedro.rodrigues@dep.uminho.pt (P.V.R.); avm@dep.uminho.pt (A.M.)

* Correspondence: rosa_batista@fisica.uminho.pt (R.M.F.B.); belsley@fisica.uminho.pt (M.B.)

Abstract: This study describes the synthesis, and characterization of lead-free organic ferroelectric perovskite *N*-methyl-*N*′-diazabicyclo[2.2.2]octonium)-ammonium trichloride (MDABCO-NH_4Cl_3). The electrospinning technique was employed to obtain nanofibers embedded with this perovskite into PVC polymer for hybrid fiber production. The dielectric, piezoelectric and pyroelectric properties of these fibers were carefully examined. From measurements of the dielectric permittivity temperature and frequency dependence, together with the pyroelectric results, a transition from a high temperature paraelectric to a ferroelectric phase that remained down to room temperature, was found to occur at 438 K. A pyroelectric coefficient as high as 290 μC K^{-1} m^{-2}value obtained is within the same order of magnitude as that reported for MDABCO-NH_4I_3 and the semiorganic ferroelectric triglycine sulfate (TGS). The hybrid nanofibers exhibited good morphological characteristics and demonstrated very good piezoelectric properties. Specifically, a piezoelectric coefficient of 42 pC/N was obtained when a periodical force of 3 N was applied. The performance of these fibers is on par with materials discussed in the existing literature for fabrication of nano energy harvesting generators. Importantly, the perovskite nanocrystals within the fibers not harmed by oxidation, making them a promising environmentally friendly platform for flexible energy harvesting.

Keywords: organic perovskite; electrospinning; fibers; piezoelectricity; pyroelectricity; nano energy harvesting

1. Introduction

Ferroelectrics are crystalline materials that simultaneously exhibit pyro-electricity and piezoelectricity due to their structure displaying spontaneous polarization, which can be reversed by the application of a static electric field. Ferroelectrics must crystallize in one of the ten crystallographic polar point groups.

Among all ferroelectrics, the best-known and widely studied family is the inorganic metal oxides known as perovskites of type ABX_3 (where A and B are metal cations, and X is an oxide anion). Examples include strontium titanate ($SrTiO_3$), barium titanate ($BaTiO_3$), lead titanate ($PbTiO_3$), and lithium niobate ($LiNbO_3$) [1]. Lead-free inorganic perovskites are wide-bandgap materials that have recently produced encouraging results as UV light photodetectors. In particular, their piezoelectric and pyroelectric properties have the potential to enhance the photoelectric conversion process [2–4].

 doi:10.20944/preprints202402.0436.v1

Hybrid perovskites represent a novel category of ferroelectric crystals that hold significant importance, not only for their crystallographic properties but also for their environmentally friendly nature. Unlike their inorganic counterparts, these semi-organic ferroelectrics offer several notable advantages. Synthesizing them at room temperature is possible, and they exhibit greater flexibility and reduced weight. Additionally, they showcase remarkable structural variability, which leads to highly tunable properties. Because of their unique qualities, hybrid perovskites have become a crucial area of research, especially for their potential as replacements for inorganic materials in piezoelectric and pyroelectric technologies [5–8].

Pyroelectrics, a distinctive subset of ferroelectrics, are crystalline polar compounds characterized by their ability to undergo a polarization change in response to variations in temperature. This unique property allows them to convert temperature fluctuations into an electric current. As a result, pyroelectrics find valuable applications in areas such as infrared detection, energy harvesting processes, and thermal imaging.

An illustrative example of a semi-organic ferroelectric is triglycine sulfate (TGS), which possesses a notable pyroelectric coefficient (p) of 306 μC/m² K. This coefficient is observed at the ferroelectric-paraelectric transition temperature of 38ºC, showcasing the material's capacity to generate an electric charge in response to temperature changes [5].

Ferroelectrics, crystalline materials that exhibit both pyroelectricity and piezoelectricity, have enormous technological significance. Since the discovery of the first semi-organic ferroelectric, Rochelle salt or sodium potassium tartrate tetrahydrate [$KNaC_4H_4O_6$ ($4H_2O$)], by Valasek in 1920, these materials have been a focal point of fundamental and applied research [6,7].

Inorganic perovskites of the ABX_3 type (where A and B are metal cations, and X is typically an oxide anion) form a well-established family of solid-state crystalline compounds. These materials have found extensive applications in the fabrication of capacitors, sensors, actuators, and various other devices. Notable examples include metal oxides such as strontium titanate ($SrTiO_3$), barium titanate ($BaTiO_3$), and lead titanate ($PbTiO_3$), as well as their solid solutions like $Pb(Zr,Ti)O_3$ (PZT), niobates such as PZN ($PbZn_{1/3}Nb_{2/3}O_3$), ($PbMg_{1/3}Nb_{2/3}O_3$) (PMN), and lithium niobate $LiNbO_3$.

These materials have been widely used in various industries due to their functional properties, combining ferroelectricity with non-linear optical and electro-optical effects, along with multiferroicity [8,9].

To the moment, piezoelectrics available on the market are predominantly characterized by inorganic perovskites, particularly materials based on lead zirconate titanate (PZT), along with polymers such as polyvinylidene difluoride (PVDF) and its derivatives, such as PVDF-TrF [10,11].

However, because of the inherent lead toxicity, lead-based ferroelectrics have become a significant environmental concern. These apprehensions have spurred active research aimed at substituting one of the ions A or X within the perovskite-type materials with a molecular building unit [12,13].

Semi-organic crystalline materials for optoelectronic applications, proving to be competitive with their inorganic counterparts. These semi-organic ferroelectrics offer several advantages over inorganic materials. Notably, researchers can synthesize these semi-organic ferroelectrics at room temperature, and they offer greater flexibility and reduced weight. Additionally, they display remarkable structural variability, resulting in highly tunable properties. As a result, they have become a focal point of research for their potential application as piezoelectric and pyroelectric materials, aiming to replace traditional inorganic counterparts [14–17].

Crucially, the pursuit of lead-free alternatives gained momentum with the discovery of highly efficient solar cells utilizing methylammonium lead halide perovskites. This breakthrough prompted the exploration of lead-free HOIPs, a recently discovered and highly promising family within the perovskite domain [18–23].

A recently discovered lead-free organic-inorganic perovskite is (N-methyl-N'-diazabicyclo[2.2.2]octonium)-ammonium triiodide, MDABCO-NH_4I_3. This material has a remarkable spontaneous polarization of 22 μC/cm², very close to that of barium titanate (approximately 26 μC/cm²). With a ferroelectric-paraelectric phase transition occurring at 448 K and exhibiting multiple

 doi:10.20944/preprints202402.0436.v1

polarization directions, MDABCO-NH_4I_3 has convincing attributes for applications in flexible optoelectronic devices [24,25].

The fabrication of nanoscale structures has received increasing attention because of their size-dependent properties. One-dimensional structures, including nanowires, nanotubes and nanofibers, represent the smallest dimensional entities that exhibit innovative properties with significant potential applications in various fields, such as electronics, photonics, sensing and energy harvesting.

Among the various techniques available, electrospinning has become a well-established method for creating micro- and nanoscale fibers, characterized by a high surface-to-volume ratio. This process results in the formation of mats measuring several square centimeters, made up of multifunctional nanostructured materials. These materials are derived from precursor polymer solutions mixed with functional nanoparticles under the influence of intense static electric fields [26–30].

Furthermore, the anisotropic shape and substantial surface area ratio of nanofibers contribute significantly to increasing their mechanical strength and flexibility. In this context, the exploration of nanoscale ferroelectrics with a perovskite structure appears to be a particularly promising and key area of research [14,31].

An interesting application of functional electrospun fibers is the collection of electrical nano energy at low frequencies through the piezoelectric effect. This phenomenon is driven by the polarization induced by the deformation of the material [32].

Piezoelectric nanogenerators, commonly referred to as PENGs, hold promise for powering low-energy devices. An illustrative example involves the utilization of a semi-organic perovskite in a PENG, as reported for methylammonium lead iodide ($CH_3NH_3PbI_3$) incorporated into PVDF polymer fibers formed via electrospinning. This configuration yielded an output voltage of approximately 220 mV at 4 Hz, with an applied force of approximately 7.5 N. Notably, it generated a maximum output power of 0.8 mW/m² [33].

In this manuscript, electrospun nanofibers incorporating MDABCO-NH_4Cl_3 perovskite demonstrate their potential as lead-free piezoelectric nanogenerators (PENGs) for efficient mechanical energy harvesting. Specifically, when applied to poly(vinyl chloride) (PVC) polymer, these nanofibers yield a piezoelectric coefficient of 42 pC/N under the influence of periodic mechanical forces. Notably, the pyroelectric coefficient of polycrystalline MDABCO-NH_4I_3 within electrospun fibers has the same order of magnitude as the hybrid ferroelectric triglycine sulfate (TGS).

2. Materials and Methods

2.1. Materials and Nanofibers Preparation

Following the synthetic procedure outlined by Yu-Meng You and Ren-Gen Xiong [24], MDABCO-NH_4Cl_3 was synthesized. The precursor (MDABCO)I was also synthesized according to the method reported by Kreuer et al. [34]. The resulting MDABCO-NH_4Cl_3 crystals were then ground in a mortar and sieved to a size smaller than 40 μm.

All chemicals and solvents, obtained from Sigma-Aldrich (Schenlldorf, Germany), were used without any further purification. Polyvinyl chloride (PVC), with a high molecular weight and a density of 1.40 g/ml, was purchased from Janssen (Beerse, Belgium). To prepare the 10% PVC electrospinning precursor solution, the pellets were dissolved in a solvent mixing system of 5 mL of tetrahydrofuran (THF) and dimethylformamide (DMF) in a 50:50 (v/v) ratio. After complete dissolution, MDABCO-NH_4Cl_3, in a ratio of 1:5 by weight, was added in small portions, and the resulting solution was stirred for several hours under ambient conditions before the electrospinning process. The precursor solution was then loaded into a 5 mL syringe, with its needle (0.5 mm outer diameter and 0.232 mm inner diameter) connected to the anode of a high-voltage power supply (Spellmann CZE2000).

The conventional electrospinning technique produced the nanofibers, configured to produce oriented fiber mats. Essentially, the equipment used consists of four principal components: a high-voltage power supply, a precise syringe pump, a syringe fitted with a metal needle (spinneret) and a drum collector connected to a motor speed controller. The power supply is connected to both the

 doi:10.20944/preprints202402.0436.v1

spinneret and the drum collector. The syringe pump regulates and controls the flow rate of the polymer solution as it consistently extrudes through the spinneret. An aluminum foil attached to the collector, amasses the fibers produced. Our electrospinning apparatus, a E-Fiber EF100 (Leonardino Srl / SKE Research Equipment®, Milan, Italy) was designed with a horizontal configuration geometry.

Nanofibers composed of PVC polymer with embedded MDABCO-NH_4Cl_3 perovskite were successfully fabricated. As a reference, nanofibers using a solution of pure PVC polymer were also electrospun. In both cases, employing polymers containing MDABCO-NH_4Cl_3 and reference solutions, a voltage of 20 kV was applied between the tip and the collector. The solution flow rate and the needle-to-collector distance were maintained at 0.18-0.20 mL/h and 13 cm, respectively.

2.2. Scanning Electron Microscopy (SEM)

The investigation into the morphology, size, and shape of MDABCO-NH_4Cl_3 perovskite nanofibers utilized a Nova Nano SEM 200 scanning electron microscope (FEI Company, Hillsboro, Oregon, United States). The instrument operated at an accelerating voltage of 10 kV. We deposited nanofibers on a silica surface that we had previously coated with a thin film (10 nm thickness) of Au-Pd (80-20 weight %). This deposition was achieved using a high-resolution sputter cover, 208HR Cressington Company (Watford, England UK), coupled with a Cressington MTM-20 high-resolution thickness controller.

The diameter range of the nanofibers was determined through SEM images processed with ImageJ 1.51n image analysis software (ImageJ2, NIH, https://imagej.nih.gov/ij/, accessed on 12 January 2024). To establish the average diameter and diameter distribution, measurements were conducted on 50 randomly selected nanofibers from the SEM images. We fitted the resulting fiber diameter distributions to a log-normal function.

2.3. X-ray Diffraction and Raman Spectroscopy

The investigation into the crystallinity and crystallographic orientation of MDABCO-NH_4Cl_3 within the fibers involved X-ray diffraction. θ–2θ scans were conducted, and the diffraction pattern was recorded using a Bruker D8 Discover X-ray diffractometer (Bruker company, Billerica, Massachusetts, USA) equipped with Cu-Kα radiation (wavelength of 1.5406 Å).

2.4. Dielectric spectroscopy

The dielectric properties of MDABCO-NH_4Cl_3 crystals and were assessed through impedance spectroscopy within the temperature range of 300-450 K and a frequency span of 100 Hz – 1 MHz. Complex permittivity, denoted as $\varepsilon=\varepsilon'-i\varepsilon''$, where ε and ε'' represent the real and imaginary components, respectively, were determined based on the measured capacitance (C) and loss tangent (tan δ), utilizing the equations:

$$C = \varepsilon'\varepsilon_0(A/d) \qquad \text{and} \qquad \tan\delta = \varepsilon''/\varepsilon'$$

In these equations, A signifies the electric contact area, and d denotes the thickness of the fiber mat. The experimental setup involved the samples forming a parallel-plate capacitor included in an LCR network. The aluminum foil, utilized as the substrate for collecting the fiber mats, served as the bottom electrode, while the top electrode was the base of a cylindrical metal contact with an approximate diameter of 10^{-2} m. Measurements were conducted using a Wayne Kerr 6440A (Wayne kerr Electronics, London, UK) precision component analyzer, along with dedicated computer software for data acquisition. Shielded test leads were employed to mitigate parasitic impedances resulting from connecting cables. Temperature-dependent measurements were executed at a rate of 2 °C/min, facilitated by a Polymer Labs PL706 PID controller (Polymer Labs, Los Angeles, California USA) and furnace.

 doi:10.20944/preprints202402.0436.v1

2.5. Pyroelectric Measurements

Pyroelectricity results from the temperature-dependent nature of spontaneous polarization, in which changes in temperature induce an electric field from changes in the intrinsic dipoles. The surface layer of free charges counteracts this electric field. The key parameter that characterizes this phenomenon is the pyroelectric coefficient, denoted by the rate of change of spontaneous polarization ($p = dPs/dT$). Measuring the change in polarization involves monitoring the pyroelectric current ($I = A(dPs/dT)(dT/dt)$) using a Keithley 617 electrometer (Keithley Instruments GmbH, Landsberg, Germany). Here, A represents the area of the electrode and dT/dt means the rate of temperature change. These measurements were carried out using a capacitor geometry under short-circuit conditions.

2.6. Piezoelectric Measurements

The piezoelectric output voltage and current of the fibers were measured across a 100 MΩ load resistance connected to a low-pass filter. Subsequently, the signals were passed through a low-noise preamplifier (SR560, Stanford Research Systems, Stanford, CA, USA) before being recorded with a digital storage oscilloscope (Agilent Technologies DS0-X-3012A, Waldbronn, Germany). Periodic applied mechanical forces generated by a vibration generator (model: SF2185, Frederiksen Scientific, Olgod, Denmark) drove the fiber array sample, with dimensions of (30 × 40) mm² and a thickness of 200 µm. A signal generator (model: 33120A, Hewlett Packard, Palo Alto, California, U.S.A.) controlled the frequency set to be 3 Hz. The applied forces were calibrated using a force-sensing resistor (FSR402, Interlink Electronics Sensor Technology, Graefelfing, Germany). The sample, fixed on a stage, experienced uniform and perpendicular application of forces over its surface area.

3. Results and discussion

3.1. Dielectrics

The frequency dependence of the electric permittivity was measured between room temperature and 453 K for the polycrystalline MDABCO-NH_4Cl_3 sample. Figure 1a,b show the real and imaginary components of the dielectric permittivity, respectively. The dielectric constant (real component of the permittivity) initially presents a sharp drop in the low-frequency region and then attains a slower decrease at high frequencies. On the other hand, two maxima, marked with the A and B letters in Figure 1b, are observed in the imaginary component of the electric permittivity, which are characteristic of the presence of two dielectric relaxations. One occurs above 10 kHz (A relaxation) and the other occurs in the 10 Hz – 1 kHz frequency region (B relaxation). These relaxations are further observed in ε′, by the appearance of two plateaus in the frequency intervals associated with the A and B maxima. The rise in the dielectric constant values at the low-frequency end (Figure 1a), is influenced by the Maxwell–Wagner–Sillars polarization that occurs at the nanoscale, where the charge carriers can be blocked at the inner dielectric boundary layers or interfaces between grains in the polycrystalline MDABCO-NH_4Cl_3 sample [35].

The frequency of the maxima of the imaginary component of the dielectric permittivity (f_m) is related to the relaxation time (τ) of the process by the equation $2\pi f_m \tau = 1$. The frequency of the maxima follows a thermally activated Arrhenius type behavior described by the equation [35]:

$$f_m = f_{m0} \exp\left(-\frac{E}{k_B T}\right) \quad (1)$$

Where f_m is the frequency of the maxima, f_{m0} is a constant, k_B is the Boltzman constant and E is the activation energy of the process. Taking the logarithm of equation (1) a linear dependence results which can be fit with a straight line according to the expression $\ln(f_m) = \ln(f_{m0}) - \frac{E}{k_B T}$: The inset of 1b) shows the linear fits to the graphics of $\ln(f_m)$ as a function of the inverse of the temperature for both relaxations. From the fits, the corresponding activation energy values were obtained, giving E_A = 0.47 eV and E_B = 0.086 eV.

 doi:10.20944/preprints202402.0436.v1

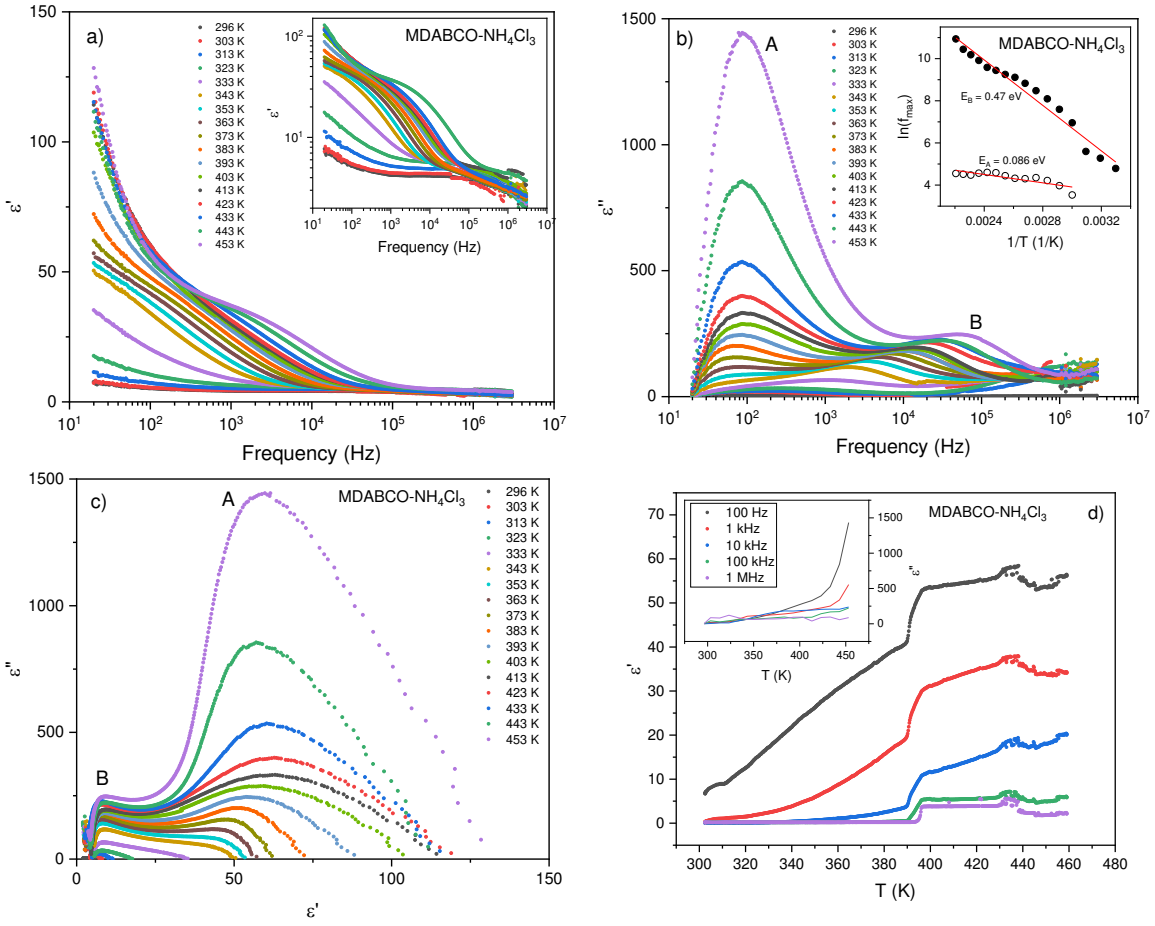

Figure 1. Frequency dependence of the **a)** real part and of the **b)** imaginary part of the dielectric permittivity polycrystalline MDABCO-NH_4Cl_3. The inset of figure **b)** shows the logarithm of the frequency of the maximum of the relaxations marked with A and B in ε'', versus the inverse of the temperature. The straight lines are fits to the curves, to obtain the corresponding activation energies. In **c)** is the Cole-Cole plot and in **d)** the temperature dependence of the real and imaginary components of the electric permittivity of the sample.

Figure 1d shows the temperature dependence of the real and imaginary (inset) parts of the electric permittivity of MDABCO-NH_4Cl_3. An overall increase of the real and imaginary permittivity is observed, with increasing temperature, reflecting the increasing thermal energy available to the system. However, a change of behavior is observed above ~398 K (a step-like change) consistent with the stabilization of a ferroelectric phase, and another (a peak) is seen at ~438 K which might be assigned to a ferroelectric-paraelectric phase transition, reported previously for MDABCO-NH_4I_3 analog. Both dielectric changes occur at temperatures where anomalies are observed in the DSC measurements (Figure S1). Accordingly, the curves in Cole-Cole plots, Figure 1c show that sharply and significant maxima occur for temperatures above 383 K.

3.2. Pyroelectricity

The pyroelectric coefficient was measured on a polycrystalline sample (a pellet) of MDABCO-NH_4Cl_3 perovskite until the Curie temperature, as shown in Figure 2. The maximum value achieved is around 290 μC K^{-1} m^{-2}. The maximum occurs in the temperature region 398 – 426 K at temperatures where there is a change of slope in the real and imaginary components of the electric permittivity, as shown in Figure 1d. This indicates the presence of structural changes inside the MDABCO-NH_4Cl_3 sample and associated with the phase transition reported for this perovskite family. The pyroelectric coefficient value obtained is within the same order of magnitude as that reported for MDABCO-NH_4I_3 and the state-of-the-art semiorganic ferroelectric triglycine sulfate (TGS) single crystal,

 doi:10.20944/preprints202402.0436.v1

reported to be respectively 194×10^{-6} $Cm^{-2}k^{-1}$ and 306×10^{-6} $Cm^{-2}k^{-1}$ at the ferroelectric-paraelectric phase transition [36]. The second maximum occurring in the temperature interval 431– 440 K is also consistent with the second anomaly observed in the temperature dependence of the electric permittivity (Figure 1d) and in the DSC measurements (Figure S1).

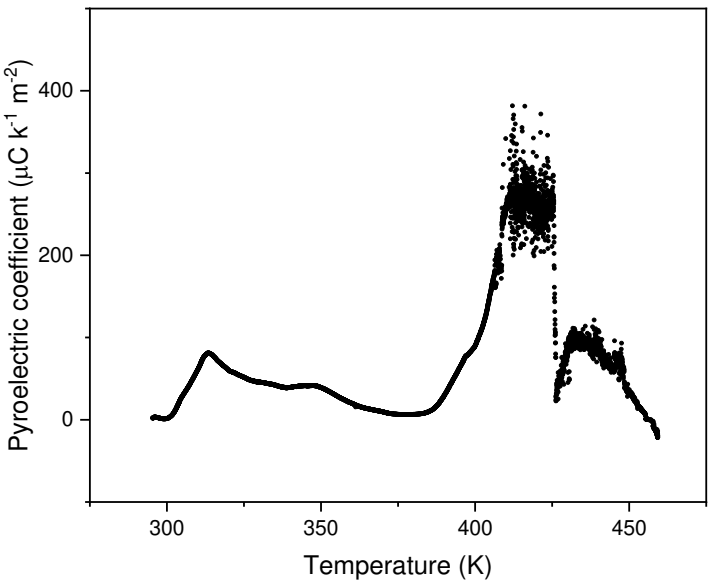

Figure 2. Pyroelectric coefficient as a function of the temperature of MDABCO-NH_4Cl_3, measured on heating.

3.3. Piezoelectric Voltage and Current, and Effective Piezoelectric Coefficients in Fibers

The piezoelectric behavior of electrospun nanofiber mats fabricated from MDABCO-NH_4Cl_3@PVC was investigated in this study. At a frequency of 3 Hz and an applied force of 3 N, Voc reaches 12 V for the Piezoelectric Nanogenerator (PENG) formed by the MDABCO-NH_4Cl_3@PVC nanofiber mat. Note that low frequencies, such as 3 Hz, allow the generator to return to its original microscopic configuration before the next force is applied.

The charge generated by the piezoelectric mat, calculated from Q = ∫Idt (C), amounts to 786 pC for the MDABCO-NH_4Cl_3@PVC mat, considering a material response time of approximately 10^{-3} s, the maximum Isc obtained of 786 nA. The effective piezoelectric coefficient, calculated as d_{eff} = Q/F (pCN^{-1}), for the nanofiber mat under a periodically applied force of 3 N is 42 pCN^{-1} for MDABCO-NH_4Cl_3@PVC. Comparatively, the piezoelectric coefficient reported for a single MDABCO-NH_4I_3 crystal is d_{33} = 14 pCN^{-1} along the [1 1 1] direction of the crystal [24]. Therefore, the piezoelectric coefficient for the hybrid system formed by MDABCO-NH_4Cl_3 nanocrystals embedded in PVC fibers is one 3 times higher. It is important to note that this hybrid perovskite PENG exhibits a small contribution from the piezoelectric polymer, which is piezoelectric (d_{31}~1.5 pCN^{-1}) [37].

This result aligns with the very high effective piezoelectric coefficient displayed by electrospun fibers incorporating active organic piezoelectric materials, as reported previously for nonlinear optical organic crystal derivatives of nanocrystalline push–pull nitroaniline molecules and di-phenylalanine dipeptides when embedded in nano and microfibers fabricated by the electrospinning technique [38–40].

Calculating the peak power density, P = Isc/A (μWm^{-2}) (where A is the area of the electrode) delivered by the MDABCO-NH_4Cl_3@PVC nanofiber mat yields 1960 μWm^{-2}, which is two orders of magnitude higher than that reported for methylammonium lead iodide ($CH_3NH_3PbI_3$) embedded into poly(vinylfluoride) (PVDF) nanofibers, reported to be 12 μWm^{-2} for Rl = 10 MΩ [33].

Moreover, the MDABCO-NH_4Cl_3@PVC piezoelectric generator can deliver a peak power density comparable to that achieved for electrically poled MDABCO-NH_4I_3 films deposited on a polyimide

 doi:10.20944/preprints202402.0436.v1

substrate after a preheating treatment up to 140°C. Here, the piezoelectric generator delivered a peak power density of 2000 μWm^{-2} under an Rl = 250 MΩ [41]. Therefore, the electrospun-doped fiber mat can achieve a high peak power density without the need for electrical polling or a previous heating treatment, providing a significant advantage.

In this work, we demonstrate that incorporating the organic lead-free perovskite MDABCO-NH_4Cl_3 into electrospun PVC fibers, processed at room temperature without poling, is an easy and straightforward method for fabricating piezoelectric generators using lead-free perovskite nanocrystals as active materials.

Furthermore, the piezoelectric voltage coefficient (g_{eff}), an essential quantity for quantifying the performance of a material for integration as a piezoelectric sensor, was calculated for our electrospun fiber mats. For MDABCO-NH_4Cl_3@PVC, $\varepsilon' = 0.0145$ at 100 Hz, and $g_{eff} = 3.6\ VmN^{-1}$. This extremely high piezoelectric voltage coefficient is one order of magnitude higher than that displayed by a polyvinylidene fluoride (PVDF) polymer thin film ($g_{eff} = 0.29\ VmN^{-1}$) [42,43] and more than five times higher than that exhibited by the layered lead perovskite (4-aminotetrahydropyran)2$PbBr_4$ ($g_{eff} = 0.67\ VmN^{-1}$) [14].

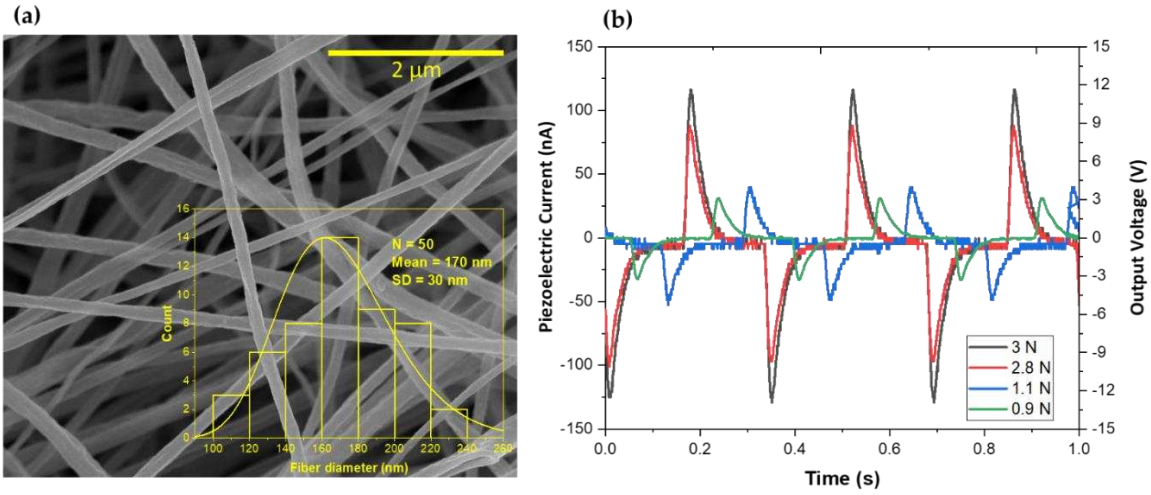

Figure 3. (a) SEM image at magnification level 50,000× and the respective fiber diameter distribution histogram for MDABCO-NH_4Cl_3@PVC fiber mat. The logarithmic normal distribution is represented by the yellow curve, which was generated using the mean and standard deviation of the data; **(b)** Output voltage and piezoelectric current as a function of time from MDABCO-NH_4Cl_3 incorporated into PVC polymer nanofibers.

5. Conclusions

The synthesis and characterization of MDABCO-NH_4Cl_3 crystals presented in this study offer valuable information on the potential applications of lead-free organic ferroelectric perovskites. The transition from a high-temperature paraelectric structure to a ferroelectric phase observed at 432 K means that the material is suitable for room-temperature ferroelectric applications. Moreover, the pyroelectric coefficient value obtained for MDABCO-NH_4Cl_3 is within the same order of magnitude as that reported for MDABCO-NH_4I_3 and the semiorganic ferroelectric triglycine sulfate (TGS), which are respectively $194\times10^{-6}\ Cm^{-2}k^{-1}$ and $306\times10^{-6}\ Cm^{-2}k^{-1}$ at the ferroelectric-paraelectric phase transition.

The successful incorporation of MDABCO-NH_4Cl_3 into PVC nanofibers, together with the observation of good morphological characteristics, underlines the feasibility of using these materials in practical devices. The piezoelectric properties demonstrated, with a measured piezoelectric coefficient of 42 pC/N under a periodic force of 3 N, and further highlights the material's potential for energy harvesting applications.

Supplementary Materials: The following supporting information can be downloaded at the website of this paper posted on Preprints.org.

Author Contributions: Conceptualization, R.M.F.B. and E.M.G.; investigation, R.M.F.B., B.S., J.O., B.A., C.C., P.V.R., A.M. and M.B.; writing—original draft preparation, R.M.F.B. and E.M.G.; writing—review and editing, R.M.F.B., E.M.G., B.A. and M.B.; supervision, R.M.F.B. and E.M.G.; project administration, R.M.F.B. and E.M.G.; funding acquisition, R.M.F.B., B.A., M.B. and E.M.G. All authors have read and agreed to the published version of the manuscript.

Funding: This research was funded by Fundação para a Ciência e Tecnologia through FEDER (European Fund for Regional Development)-COMPETE-QREN-EU (ref. UID/FIS/04650/2013 and UID/FIS/04650/2019); E-Field—"Electric-Field Engineered Lattice Distortions (E-FiELD) for optoelectronic devices", ref.: PTDC/NAN-MAT/0098/2020; Gemis—"Graphene-enhanced electro-magnetic interference shielding", Ref.: POCI-01-0247-FEDER-045939 and "Non-linear phononics: Manipulating the hidden quantum phases and dynamical multiferroicity", Ref. 2022.03564.PTDC.

Institutional Review Board Statement: This study did not involve humans or animals.

Informed Consent Statement: This study did not involve humans or animals.

Acknowledgments: We acknowledge national funds (OE), through FCT − Fundação para a Ciência e a Tecnologia, I.P., in the scope of the framework contract foreseen in the numbers 4, 5 and 6 of article 23 of the Decree-Law 57/2016, of August 29, changed by Law 57/2017, of July 19. DL 57/2016/CP1377/CT0064 (DOI: 10.54499/DL57/2016/CP1377/CT0064).

Conflicts of Interest: The authors declare no conflict of interest.

References

1. Lines, M.E.; Glass, A.M. Principles and applications of ferroelectrics and related materials; Oxford university press: 2001.
2. Zhou, X.; Ke, Q.; Tang, S.; Luo, J.; Lu, Z. Ultraviolet photodetectors based on ferroelectric depolarization field. *Journal of Energy Chemistry* **2023**, *77*, 487-498, doi:https://doi.org/10.1016/j.jechem.2022.11.021.
3. Zhou, X.; Lu, Z.; Zhang, L.; Ke, Q. Wide-bandgap all-inorganic lead-free perovskites for ultraviolet photodetectors. *Nano Energy* **2023**, *117*, 108908, doi:https://doi.org/10.1016/j.nanoen.2023.108908.
4. Martínez-Goyeneche, L.; Gil-Escrig, L.; Susic, I.; Tordera, D.; Bolink, H.J.; Sessolo, M. Narrowband Monolithic Perovskite–Perovskite Tandem Photodetectors. *Adv Opt Mater* **2022**, *10*, 2201047.
5. Bowen, C.R.; Taylor, J.; LeBoulbar, E.; Zabek, D.; Chauhan, A.; Vaish, R. Pyroelectric materials and devices for energy harvesting applications. *Energy & Environmental Science* **2014**, *7*, 3836-3856, doi:10.1039/C4EE01759E.
6. Valasek, J. Properties of Rochelle Salt Related to the Piezo-electric Effect. *Physical Review* **1922**, *20*, 639-664, doi:10.1103/PhysRev.20.639.
7. Valasek, J. Piezo-Electric and Allied Phenomena in Rochelle Salt. *Physical Review* **1921**, *17*, 475-481, doi:10.1103/PhysRev.17.475.
8. Lines, M.E.; Glass, A.M. *Principles and Applications of Ferroelectrics and Related Materials*; Oxford University Press: Oxford, 2001; p. 694.
9. Scott James, F.; Paz de Araujo Carlos, A. Ferroelectric Memories. *Science* **1989**, *246*, 1400-1405, doi:10.1126/science.246.4936.1400.
10. Zhao, Z.; Dai, Y.; Dou, S.X.; Liang, J. Flexible nanogenerators for wearable electronic applications based on piezoelectric materials. *Materials Today Energy* **2021**, *20*, 100690, doi:https://doi.org/10.1016/j.mtener.2021.100690.
11. Sezer, N.; Koç, M. A comprehensive review on the state-of-the-art of piezoelectric energy harvesting. *Nano Energy* **2021**, *80*, 105567, doi:https://doi.org/10.1016/j.nanoen.2020.105567.
12. Cross, E. Lead-free at last. *Nature* **2004**, *432*, 24-25, doi:10.1038/nature03142.
13. Saito, Y.; Takao, H.; Tani, T.; Nonoyama, T.; Takatori, K.; Homma, T.; Nagaya, T.; Nakamura, M. Lead-free piezoceramics. *Nature* **2004**, *432*, 84-87, doi:10.1038/nature03028.
14. Chen, X.-G.; Song, X.-J.; Zhang, Z.-X.; Li, P.-F.; Ge, J.-Z.; Tang, Y.-Y.; Gao, J.-X.; Zhang, W.-Y.; Fu, D.-W.; You, Y.-M.; et al. Two-Dimensional Layered Perovskite Ferroelectric with Giant Piezoelectric Voltage Coefficient. *J Am Chem Soc* **2020**, *142*, 1077-1082, doi:10.1021/jacs.9b12368.

15. Guo, T.-M.; Gong, Y.-J.; Li, Z.-G.; Liu, Y.-M.; Li, W.; Li, Z.-Y.; Bu, X.-H. A New Hybrid Lead-Free Metal Halide Piezoelectric for Energy Harvesting and Human Motion Sensing. *Small* **2022**, *18*, 2103829, doi:https://doi.org/10.1002/smll.202103829.
16. Zhang, H.-Y.; Tang, Y.-Y.; Shi, P.-P.; Xiong, R.-G. Toward the Targeted Design of Molecular Ferroelectrics: Modifying Molecular Symmetries and Homochirality. *Accounts Chem Res* **2019**, *52*, 1928-1938, doi:10.1021/acs.accounts.8b00677.
17. Li, W.; Wang, Z.; Deschler, F.; Gao, S.; Friend, R.H.; Cheetham, A.K. Chemically diverse and multifunctional hybrid organic–inorganic perovskites. *Nature Reviews Materials* **2017**, *2*, 16099, doi:10.1038/natrevmats.2016.99.
18. Song, X.; Hodes, G.; Zhao, K.; Liu, S. Metal-Free Organic Halide Perovskite: A New Class for Next Optoelectronic Generation Devices. *Adv Energy Mater* **2021**, *11*, 2003331, doi:https://doi.org/10.1002/aenm.202003331.
19. Chu, L.-L.; Zhang, T.; Zhang, W.-Y.; Shi, P.-P.; Gao, J.-X.; Ye, Q.; Fu, D.-W. Three-Dimensional Metal-Free Molecular Perovskite with a Thermally Induced Switchable Dielectric Response. *The Journal of Physical Chemistry Letters* **2020**, *11*, 1668-1674, doi:10.1021/acs.jpclett.9b03556.
20. You, Y.-M.; Liao, W.-Q.; Zhao, D.; Ye, H.-Y.; Zhang, Y.; Zhou, Q.; Niu, X.; Wang, J.; Li, P.-F.; Fu, D.-W.; et al. An organic-inorganic perovskite ferroelectric with large piezoelectric response. *Science* **2017**, *357*, 306-309, doi:10.1126/science.aai8535.
21. Saparov, B.; Mitzi, D.B. Organic–Inorganic Perovskites: Structural Versatility for Functional Materials Design. *Chemical Reviews* **2016**, *116*, 4558-4596, doi:10.1021/acs.chemrev.5b00715.
22. Kamat, P.V.; Bisquert, J.; Buriak, J. Lead-Free Perovskite Solar Cells. *ACS Energy Letters* **2017**, *2*, 904-905, doi:10.1021/acsenergylett.7b00246.
23. Boix, P.P.; Agarwala, S.; Koh, T.M.; Mathews, N.; Mhaisalkar, S.G. Perovskite Solar Cells: Beyond Methylammonium Lead Iodide. *The Journal of Physical Chemistry Letters* **2015**, *6*, 898-907, doi:10.1021/jz502547f.
24. Ye, H.-Y.; Tang, Y.-Y.; Li, P.-F.; Liao, W.-Q.; Gao, J.-X.; Hua, X.-N.; Cai, H.; Shi, P.-P.; You, Y.-M.; Xiong, R.-G. Metal-free three-dimensional perovskite ferroelectrics. *Science* **2018**, *361*, 151-155, doi:10.1126/science.aas9330.
25. Wang, H.; Liu, H.; Zhang, Z.; Liu, Z.; Lv, Z.; Li, T.; Ju, W.; Li, H.; Cai, X.; Han, H. Large piezoelectric response in a family of metal-free perovskite ferroelectric compounds from first-principles calculations. *npj Computational Materials* **2019**, *5*, 17, doi:10.1038/s41524-019-0157-4.
26. Doshi, J.; Reneker, D.H. Electrospinning process and applications of electrospun fibers. *Journal of Electrostatics* **1995**, *35*, 151-160, doi:https://doi.org/10.1016/0304-3886(95)00041-8.
27. Reneker, D.H.; Chun, I. Nanometre diameter fibres of polymer, produced by electrospinning. *Nanotechnology* **1996**, *7*, 216 - 223.
28. Ramakrishna, S.; Fujihara, K.; Teo, W.-E.; Yong, T.; Ma, Z.; Ramaseshan, R. Electrospun nanofibers: solving global issues. *Materials Today* **2006**, *9*, 40-50, doi:https://doi.org/10.1016/S1369-7021(06)71389-X.
29. Isakov, D.V.; de Matos Gomes, E.; Vieira, L.G.; Dekola, T.; Belsley, M.S.; Almeida, B.G. Oriented single-crystal-like molecular arrangement of optically nonlinear 2-methyl-4-nitroaniline in electrospun nanofibers. *Acs Nano* **2011**, *5*, 73-78.
30. Richard-Lacroix, M.; Pellerin, C. Molecular Orientation in Electrospun Fibers: From Mats to Single Fibers. *Macromolecules* **2013**, *46*, 9473-9493, doi:10.1021/ma401681m.
31. Rørvik, P.M.; Grande, T.; Einarsrud, M.-A. One-Dimensional Nanostructures of Ferroelectric Perovskites. *Adv Mater* **2011**, *23*, 4007-4034, doi:https://doi.org/10.1002/adma.201004676.
32. Isakov, D.; de Matos Gomes, E.; Almeida, B.; Kholkin, A.L.; Zelenovskiy, P.; Neradovskiy, M.; Shur, V.Y. Energy harvesting from nanofibers of hybrid organic ferroelectric dabcoHReO4. *Appl Phys Lett* **2014**, *104*, 032907, doi:10.1063/1.4862437.
33. Sultana, A.; Ghosh, S.K.; Alam, M.M.; Sadhukhan, P.; Roy, K.; Xie, M.; Bowen, C.R.; Sarkar, S.; Das, S.; Middya, T.R.; et al. Methylammonium Lead Iodide Incorporated Poly(vinylidene fluoride) Nanofibers for Flexible Piezoelectric–Pyroelectric Nanogenerator. *Acs Appl Mater Inter* **2019**, *11*, 27279-27287, doi:10.1021/acsami.9b04812.
34. Marino, M.G.; Kreuer, K.D. Alkaline Stability of Quaternary Ammonium Cations for Alkaline Fuel Cell Membranes and Ionic Liquids. *Chemsuschem* **2015**, *8*, 513-523, doi:10.1002/cssc.201403022.
35. Kremer, F.; Schönhals, A. *Broadband dielectric spectroscopy*; Springer Science & Business Media: 2003.

36. Ghane-Motlagh, R.; Kroener, M.; Goldschmidtboeing, F.; Danilewsky, A.N.; Woias, P. A dynamic method for the measurement of pyroelectric properties of materials. *Smart Mater Struct* **2018**, *27*, doi:Artn 084004 10.1088/1361-665x/Aac0b3.
37. Bharti, V.; Kaura, T.; Nath, R. Improved piezoelectricity in solvent-cast PVC films. *IEEE Transactions on Dielectrics and Electrical Insulation* **1995**, *2*, 1106-1110, doi:10.1109/TDEI.1995.8881940.
38. Baptista, R.M.F.; Lopes, P.E.; Rodrigues, A.R.O.; Cerca, N.; Belsley, M.S.; de Matos Gomes, E. Self-assembly of Boc-p-nitro-l-phenylalanyl-p-nitro-l-phenylalanine and Boc-l-phenylalanyl-l-tyrosine in solution and into piezoelectric electrospun fibers. *Materials Advances* **2022**, *3*, 2934-2944, doi:10.1039/D1MA01022K.
39. Baptista, R.M.F.; de Matos Gomes, E.; Raposo, M.M.M.; Costa, S.P.G.; Lopes, P.E.; Almeida, B.; Belsley, M.S. Self-assembly of dipeptide Boc-diphenylalanine nanotubes inside electrospun polymeric fibers with strong piezoelectric response. *Nanoscale Advances* **2019**, *1*, 4339-4346, doi:10.1039/C9NA00464E.
40. Bernardo, C.R.; Baptista, R.M.F.; de Matos Gomes, E.; Lopes, P.E.; Raposo, M.M.M.; Costa, S.P.G.; Belsley, M.S. Anisotropic PCL nanofibers embedded with nonlinear nanocrystals as strong generators of polarized second harmonic light and piezoelectric currents. *Nanoscale Advances* **2020**, *2*, 1206-1213, doi:10.1039/C9NA00687G.
41. Wu, H.-S.; Wei, S.-M.; Chen, S.-W.; Pan, H.-C.; Pan, W.-P.; Huang, S.-M.; Tsai, M.-L.; Yang, P.-K. Metal-Free Perovskite Piezoelectric Nanogenerators for Human–Machine Interfaces and Self-Powered Electrical Stimulation Applications. *Adv Sci* **2022**, *9*, 2105974, doi:https://doi.org/10.1002/advs.202105974.
42. Li, M.; Wondergem, H.J.; Spijkman, M.-J.; Asadi, K.; Katsouras, I.; Blom, P.W.M.; de Leeuw, D.M. Revisiting the δ-phase of poly(vinylidene fluoride) for solution-processed ferroelectric thin films. *Nat Mater* **2013**, *12*, 433-438, doi:10.1038/nmat3577.
43. Li, M.Y.; Wondergem, H.J.; Spijkman, M.J.; Asadi, K.; Katsouras, I.; Blom, P.W.M.; de Leeuw, D.M. Revisiting the delta-phase of poly(vinylidene fluoride) for solution-processed ferroelectric thin films. *Nat Mater* **2013**, *12*, 433-438, doi:10.1038/NMAT3577.
44. Baptista, R.M.F.; Moreira, G.; Silva, B.; Oliveira, J.; Almeida, B.; Castro, C.; Rodrigues, P.V.; Machado, A.; Belsley, M.; de Matos Gomes, E. Lead-Free MDABCO-NH4I3 Perovskite Crystals Embedded in Electrospun Nanofibers. *Materials* **2022**, *15*, 8397.